Research Square

Preprints are preliminary reports that have not undergone peer review.
They should not be considered conclusive, used to inform clinical practice,
or referenced by the media as validated information.

CAR-Cytotox: A Standardized Framework to Quantify Cytotoxic Potency in CAR T Cell Products

Lucija Sršen
University of Ljubljana, Faculty of Medicine
Larisa Janžič
University of Ljubljana, Faculty of Medicine
Irena Auersperger
Ljubljana University Medical Centre
Katarina Reberšek
Ljubljana University Medical Centre
Tadej Furlan
Ljubljana University Medical Centre
Enver Melkić
Ljubljana University Medical Centre
Samo Zver
Ljubljana University Medical Centre
Matjaž Sever
Ljubljana University Medical Centre
Alojz Ihan
University of Ljubljana, Faculty of Medicine
Andreja Nataša Kopitar
andreja-natasa.kopitar@mf.uni-lj.si

University of Ljubljana, Faculty of Medicine

Article

Keywords:

Posted Date: May 14th, 2026

DOI: https://doi.org/10.21203/rs.3.rs-9287376/v1

License: This work is licensed under a Creative Commons Attribution 4.0 International License. Read Full License

Additional Declarations: No competing interests reported.

Abstract

Chimeric antigen receptor (CAR) T cell therapy is a revolutionizing treatment, but its functional potency varies widely across donors, manufacturing runs, and patients. However, routine product release testing rarely measures cytotoxic competence. We introduce a standardized framework that integrates complementary readouts following 48 hour CD19-bead stimulation: degranulation by flow cytometry (CD107a), transcriptional upregulation by RT–qPCR (*BCL2, DOCK8, FHL3, GZMB, ITGB1, NKG7, PRF1, STX11, UNC13D*), and secreted effectors by multiplex immunoassay (IL-4, IL-6, IL-10, IL-17A, TNF-α, IFN-γ, soluble Fas, FasL, granzyme A, granzyme B, perforin, and granulysin). In CAR T cell products generated from 13 healthy donors and three B-ALL patients, stimulation increased CD107a, upregulated GZMB and BCL2, and elevated IFN-γ, IL-6, IL-4, and FasL. Marker fold changes are scaled between no change and the healthy-donor 90th percentile, and weighted to yield a 0–10 CAR-Cytotox score summarizing the overall cytotoxic potency of the CAR T cell product. Scores were interpreted using prespecified bands: low (0–3), moderate (3–6), or high (6–10) cytotoxicity with borderline values assigned to the higher band. The healthy-donor mean score was 4.53 ± 0.66, while patient scores were 2.14, 6.70, and 7.38, spanning low to high cytotoxicity bands. A client-side calculator implementing the CAR-Cytotox algorithm is available at https://lsrsen.github.io/CAR-Cytotox/.

1. Introduction

Chimeric antigen receptor (CAR) T cell therapy has transformed outcomes for patients with B cell malignancies, yet the functional potency of a given product remains markedly heterogeneous across donors, manufacturing runs, and individual patients. This variability arises from both biological and technical factors. The T cell starting material differs in immunophenotypic profile, differentiation state, and prior treatment exposure. Cancer therapies, including chemotherapy, immunotherapy, and other treatments, have profound effects on the immune system and can induce long-lasting alterations in T cells. In many patients, these interventions cause T cell exhaustion even before CAR T cell manufacturing begins, resulting in cells with reduced proliferative and cytotoxic potential. The manufacturing process itself further challenges cellular fitness. The *ex vivo* manufacturing process typically lasts around two weeks, during which T cells undergo activation, genetic modification, and expansion under intense cytokine and metabolic stress (1). These steps amplify pre-existing biological differences, often leading to variability in cellular composition, functional state, and overall quality of the cellular product. Despite this heterogeneity, current product testing focuses mainly on phenotypic identity, viability, and surface CAR expression (2), confirming successful engineering but not functional competence. As a result, the true cytotoxic capacity of a CAR T cell product is typically revealed only after infusion, when its biological activity becomes evident through clinical response or toxicity. The lack of early functional assessment carries clinical risk, as suboptimal products may fail to provide therapeutic benefit while exposing patients to treatment-related toxicities and delaying the opportunity to redirect them toward a more suitable treatment approach. The absence of standardized *in vitro* assays that directly evaluate functional potency limits comparability across products and manufacturing platforms and constrains efforts to optimize production and predict therapeutic efficacy.

A variety of *in vitro* assays have been developed to assess CAR T cell cytotoxicity, yet each captures only a narrow aspect of function and is subject to methodological and biological variability. Target cell killing assays, such as chromium release or flow cytometry-based co-culture assays, directly measure target cell lysis but depend heavily on the type of target cells used (3). Many target cell lines express a broad range of immunologic and cancer-associated antigens that can stimulate T cell activation independently of the CAR, leading to responses not strictly related to the CAR receptor. In addition, antigen density, co-stimulatory molecules, and intrinsic susceptibility to lysis vary substantially across target cell lines and passages, introducing variability that complicates standardization and comparability between studies. Although primary target cells may better represent the disease context, they are difficult to maintain *in vitro*, particularly in media optimized for T cell growth. Loss of viability in such cultures often reflects unfavorable growth conditions rather than CAR-dependent cytotoxicity, and pronounced inter-patient variability in malignant cell characteristics further complicates their use for standardized potency assessment. Live-cell imaging approaches provide valuable kinetic information but are resource-intensive and lack standardized analytical frameworks (4). Degranulation assays, typically measuring surface expression of CD107a (3), quantify the mobilization of lytic granules toward the cell membrane, but assess only this single compartment of cytotoxicity. They do not reveal whether key effector molecules are sufficiently produced and released to execute target cell killing. Similarly, cytokine release assays,

including ELISA or multiplex bead-based assays, provide valuable information about secretory activity but do not necessarily reflect effective cytotoxic function, as cytokine production can occur in the absence of actual target cell death or may reflect regulatory rather than effector programs (3). Transcriptional assays, such as quantitative PCR, capture gene expression dynamics following antigen recognition (3), but their relationship with cytotoxic activity is inconsistent. Functional killing occurs at the protein level, and transcriptional changes can be transient or even downregulated after activation as part of feedback regulation (5). Another limitation of all single-parameter approaches is the high baseline expression of cytotoxicity-related markers in *ex vivo* expanded CAR T cells (6, 7). Because these cells have been repeatedly activated and exposed to stressful manufacturing conditions, markers of activation, degranulation, and transcriptional activity may already be elevated before antigen encounter. As a result, small but biologically meaningful functional differences can be obscured when only one marker or readout is analyzed in isolation. Together, these limitations underscore the need for a more comprehensive and standardized framework that integrates multiple complementary assays to accurately characterize CAR T cell cytotoxic function.

Cytotoxic activity is a multifaceted process resulting from a series of tightly coordinated biological programs. Following antigen recognition, CAR T cells undergo rapid degranulation, releasing vesicles that contain cytolytic effector molecules responsible for immediate target cell killing. This is accompanied by transcriptional reprogramming that reinforces effector function and supports T cell persistence through upregulation of effector function related genes. In parallel, the secretion of effector cytokines and other regulatory mediators facilitates intercellular communication and amplifies both cytotoxic and immunomodulatory responses. Together, these functional layers define the overall cytotoxic competence of CAR T cells and underscore the importance of assessing multiple complementary dimensions of activity within a unified and standardized experimental framework.

The objective of this study was to establish a standardized framework for quantifying CAR T cell cytotoxicity that captures the multidimensional nature of their effector function. The goal was to integrate complementary aspects of CAR T cell activity, including degranulation, transcriptional adaptation, and cytokine secretion, into a single interpretable measure of functional potency. This approach aims to bridge the gap between diverse existing assays and the need for a reproducible and comparable assessment of CAR mediated cytotoxicity, supporting more accurate evaluation of product quality and therapeutic potential.

2. Methods

2.1. Study design

Thirteen healthy adult volunteers were recruited for this study. Each volunteer donated a 15 mL peripheral blood sample collected at a single time point. Peripheral blood samples from three patients diagnosed with B cell acute lymphoblastic leukemia (ALL) and treated at the Department of Hematology, University Medical Centre Ljubljana, were also obtained at the time of initial diagnosis, before therapy initiation, to minimize treatment-related effects on sample properties. Demographic and clinical data were recorded for all participants, including age, gender, treatment history, and, for patients, disease burden. The study was conducted in accordance with the Declaration of Helsinki and approved by the Ministry of Health of the Republic of Slovenia, National Medical Ethics Committee (approval code: 0120–514/2023/5), with written informed consent obtained from all participants.

2.2. Preparation of CAR T cells

Peripheral blood mononuclear cells (PBMCs) were isolated from whole blood by density-gradient centrifugation. $CD4^+$ and $CD8^+$ T lymphocytes were then purified from PBMCs by flow cytometric cell sorting using anti-human CD4 BV510 (BD Biosciences, USA) and anti-human CD8 Alexa Fluor 700 (BioLegend, USA) on a BD FACSAria III cell sorter (BD Biosciences, USA). After sorting, T cells were resuspended in growth medium (RPMI-1640 supplemented with 10% fetal bovine serum (FBS), 1% L-glutamine, 100 U/mL penicillin, 100 µg/mL streptomycin, 1 µg/mL amphotericin B) with 30 U/mL interleukin-2 (IL-2) (Gibco, Thermo Fisher Scientific, USA), and activated with anti-CD3/anti-CD28–coated magnetic beads (Gibco, Thermo Fisher Scientific, USA) at a 1:1 bead-to-cell ratio for 40 h at 37°C in 5% CO_2. After 2 days, cells were resuspended in fresh growth medium with 30 U/mL IL-2, 17 µg/mL protamine sulfate (MP Biomedicals, USA), and a lentiviral anti-CD19 CAR expression vector at multiplicity of infection (MOI) 30 (VectorBuilder, USA). The suspension was centrifuged at 180 × g for 99 min (spinoculation) and then

incubated for 40 h at 37°C in 5% CO_2. Magnetic beads were removed after 7 days. After transduction, unbound lentiviral vector was removed and cells were expanded for 8 days in growth medium supplemented with 200 U/mL IL-2. Medium was changed every 2–3 days. Following expansion, cells were transferred to fresh growth medium containing 30 U/mL IL-2 and rested for 24 h. The CAR T cell product was used for functional testing. Transduction efficiency was quantified by flow cytometry using the CD19 CAR detection reagent (Miltenyi Biotec, Germany) on a BD FACSAria III and expressed as the percentage of CAR^+ cells within T lymphocytes ($CD4^+$ and $CD8^+$) and within $CD4^+$ and $CD8^+$ subsets and reported as mean ± standard error of the mean (SEM).

2.3. Functional testing

CAR T cell cytotoxic function was assessed by stimulating cells with CD19-coated beads, followed by downstream analyses. For stimulation, streptavidin magnetic beads (MedChemExpress, USA) were coated with CD19 protein (MedChemExpress, USA) and used at 18 µg of beads per 1×10^6 cells in growth medium containing 30 U/mL IL-2. Unstimulated control was prepared identically, except without CD19-coated beads. Cell–bead suspensions were incubated for 48 hours at 37°C in 5% CO_2. After incubation, magnetic beads were removed, and cells and culture supernatants were collected. Three downstream assays (flow cytometry, real-time quantitative polymerase chain reaction (RT-qPCR), and multiplex bead-based assay) were performed to identify markers that showed statistically significant differences between CD19-stimulated CAR T cells and unstimulated controls.

2.3.1. Flow cytometry

Degranulation was quantified by measuring surface CD107a expression on $CD8^+$ CAR^+ T cells following CD19-bead stimulation. Cells were stained with CD107a FITC (BD Biosciences, USA), CD8 Alexa Fluor 700 (BioLegend, USA), and CD19 CAR Detection Reagent (Miltenyi, Germany), and events acquired on a BD FACSAria III. Table 1 details the analytes included in this study, their functional rationale, and expected change in CAR T cells. An unstimulated control was processed in parallel. Results are reported as mean ± SEM of the percentage of $CD107a^+$ cells within $CD8^+$ CAR^+ T lymphocytes for both stimulated and matched unstimulated conditions. The absolute mean increase in percentage points from the unstimulated to the stimulated condition and the fold change (stimulated/unstimulated) are also reported.

2.3.2. RT-qPCR

Total RNA was extracted using the RNeasy Plus Mini Kit (Qiagen, Germany) and quantified with the Qubit RNA Broad Range Assay (Thermo Fisher Scientific, USA) on a Qubit 4 Fluorometer (Thermo Fisher Scientific). A total of 0.2 µg of RNA was reverse-transcribed to cDNA with the High-Capacity cDNA Reverse Transcription Kit (Applied Biosystems, Thermo Fisher Scientific, USA) on a Veriti Thermal Cycler (Thermo Fisher Scientific, USA), and cDNA was stored at − 70°C until analysis. In two healthy-donor samples with limited cell input, a low-input workflow was used: direct cDNA synthesis with the SuperScript IV CellsDirect cDNA Synthesis Kit (Thermo Fisher Scientific, USA), followed by cDNA preamplification with TaqMan PreAmp Master Mix (10 cycles). Preamplified cDNA was diluted 1:5 before qPCR. Results obtained with this workflow were consistent with those from the standard extraction protocol. For qPCR, cDNA was amplified with TaqMan Fast Advanced Master Mix (Thermo Fisher Scientific, USA) and predesigned TaqMan Gene Expression Assays for *BCL2, DOCK8, FHL3, GZMB, ITGB1, NKG7, PRF1, STX11, UNC13D*, and the reference gene *HPRT1* (Thermo Fisher Scientific, USA). The analyte panel and rationale for each marker are summarized in Table 1. No-template controls (nuclease-free water) were included. Reactions were run in duplicate on a QuantStudio 5 Real-Time PCR System (Thermo Fisher Scientific, USA) according to the manufacturer's instructions. Relative expression was calculated by the $2^{-\Delta\Delta Ct}$ method with *HPRT1* as the endogenous control and the unstimulated condition as the calibrator. Results are reported as the mean ± SEM of the fold change ($2^{-\Delta\Delta Ct}$) relative to the unstimulated control. The fold increase (fold change − 1), defined as the increase from the unstimulated to the stimulated condition, is also reported.

2.3.3. Multiplex bead-based immunoassay

Cell-culture supernatants were stored at − 70°C and thawed on ice immediately before assay. Analytes (IL-4, IL-6, IL-10, IL-17A, TNF-α, IFN-γ, soluble Fas, FasL, granzyme A, granzyme B, perforin, and granulysin) were quantified using the LEGENDplex Human CD8/NK Panel, V02 (BioLegend, USA) according to the manufacturer's protocol. The selected analytes and their roles in

CAR T cell cytotoxicity are outlined in Table 1. Beads were acquired on a BD FACSCanto II flow cytometer (BD Biosciences, USA), and concentrations were calculated from standard curves (5-parameter logistic fit) using the LEGENDplex Data Analysis Software (BioLegend, USA). Supernatants from unstimulated CAR T cells were processed in parallel as unstimulated controls. Results are reported as mean ± SEM in pg/mL, along with absolute mean increases in concentration (stimulated – unstimulated) and fold changes (stimulated/unstimulated).

Table 1 Analytes used to profile CAR T cell cytotoxicity with assay methods and expected changes in CAR T cells.

Method of detection	Analyte	Role in cytotoxicity mechanisms	Expected change in CAR T cells	Ref.
Flow cytometry	CD107a (LAMP-1)	Degranulation marker, transiently externalized during lytic granule fusion with plasma membrane	Increased surface expression upon target recognition	3
RT-qPCR	BCL2	Anti-apoptotic protein, enhancing cell survival and persistence	Upregulated after the acute effector phase to support cell survival	12, 13
	DOCK8	Cytoskeletal remodeling for immune synapse organization and lytic granule polarization	Upregulated for effective immune synapse formation	19, 20
	FHL3	Adaptor protein involved in cytoskeletal organization and granule trafficking	Enhanced expression in effector T cells	18, 21
	GZMB (Granzyme B)	Effector protease inducing target-cell apoptosis	Strongly upregulated in activated CAR T cells	11
	ITGB1 (Integrin β1)	Mediates adhesion and synapse stability	Upregulated to support stable target engagement	23
	NKG7	Regulates lytic granule exocytosis and immunological synapse efficiency	Elevated during cytotoxic activation	24, 25
	PRF1 (Perforin)	Forms pores in target cell membrane for granzyme entry	Upregulated during CAR T activation and target killing	28
	STX11 (Syntaxin-11)	Controls vesicles trafficking and exocytosis	Enhanced in functional CAR T cells	31
	UNC13D (Munc13-4)	Primes lytic granules to cell membrane for exocytosis	Upregulated during activation and degranulation	32
Multiplex bead-based immunoassay	IFN-γ	Key inflammatory cytokine of T cell effector function	Elevated upon antigen angagement in activated CAR T cells	1
	TNF-α	Proinflammatory cytokine contributing to cytotoxicity and cytokine release	Increases with CAR T activation	40
	Fas	A cell-surface death receptor that triggers apoptosis upon FasL engagement	Elevated to promote activation-induced cell death	36
	FasL	Ligand commonly expressed in activated T cells to induce apoptosis of Fas-positive target cells	Upregulated during effector differentiation	36
	Granzyme A	Cytotoxic serine protease mediating target-cell death	Elevated during cytotoxic response	28
	Granzyme B	Key cytotoxic effector protease that initiates apoptosis in target cells	Highly expressed and released upon antigen recognition	28
	Perforin	Pore-forming protein enabling granzyme entry to target cells	Parallel increase with granzyme expression	28
	Granulysin	Antimicrobial and cytolytic molecule co-released with granzymes	Elevated in strongly activated cytotoxic subsets	28

IL-6	Pro-inflammatory cytokine linked to cytokine release syndrome	Elevated in activated CAR T cells	33
IL-10	Anti-inflammatory regulatory cytokine that limits excessive immune activation	Increased after activation	37
IL-4	Th2 regulatory cytokine reducing excessive cytotoxicity	Increased after CAR T cytotoxic mechanisms	35
IL-17A	Th17 pro-inflammatory cytokine supporting T cell function and persistence	Increased in activated CAR T cells	41, 43

Insert Table 1 about here.

2.4. Statistical analysis

Data from healthy donors are presented as mean ± SEM (n = 13). Normality was assessed using the Shapiro–Wilk test, and the data were considered normally distributed. RT-qPCR fold changes were compared with the unstimulated control using one-way repeated-measures ANOVA with *post-hoc* Dunnett's multiple comparisons test. Analyte concentrations from the LEGENDplex multiplex bead-based immunoassay (BioLegend, USA) were analyzed with paired t-tests and *post-hoc* Šidák-Bonferroni correction for multiple comparisons. CD107a degranulation was analyzed with a paired t-test. All tests were two-sided, and $p < 0.05$ was considered statistically significant. Analyses were performed in GraphPad Prism v10.6.1 (GraphPad Software, USA). Flow cytometry data were acquired in BD FACSDiva (BD Biosciences, USA) and analyzed in FlowJo v10 (FlowJo, LLC, USA).

2.5. CAR-Cytotox score construction

We developed a 0–10 scoring system to quantify CAR-related cytotoxicity. After completing all functional assays (flow cytometry, RT-qPCR, and multiplex bead-based immunoassay), markers whose readouts differed between CD19-stimulated and unstimulated conditions in the 13 healthy donors were identified. Weights were assigned to each marker according to predefined significance thresholds using adjusted p values ($0.05 \geq p > 0.01$: 1 point; $0.01 \geq p > 0.001$: 2 points; $0.001 \geq p$: 3 points). Non-significant markers ($p > 0.05$) were excluded from the score. For each selected marker, fold change (FC) was calculated as Stimulated/Unstimulated for flow cytometry and multiplex bead-based immunoassay, and as $2^{-\Delta\Delta Ct}$ for RT-qPCR. For each marker, FC = 1 (no change) and the healthy-donor 90th percentile ($P90$) served as the lower and upper anchors. For sample i and marker j, a normalized contribution (N) was computed as shown in Eq. 1.

$$N_{ij} = \frac{FC_{ij} - 1}{P90_j - 1} \quad (1)$$

with N_{ij} constrained to [0,1]. N_{ij} was then multiplied by the marker's weight. Contributions were summed across markers, with weights specified to sum to 10, yielding a total CAR-Cytotox score bounded between 0 (no cytotoxic activity) and 10 (very high cytotoxic activity). Scores were interpreted using prespecified bands: low (0–3), moderate (3–6), or high (6–10) cytotoxicity, with borderline values assigned to the higher band.

2.6. Score validation

Healthy donor and patient data were used to evaluate the stability and robustness of the CAR-Cytotox score.

2.6.1. Leave-One-Out jackknife

A leave-one-out (LOO) jackknife was applied to test the stability of the $P90$ anchors and assess single-donor influence on CAR-Cytotox scores. Per-marker $P90$ anchors were recalculated 13 times, each time omitting one healthy donor. After each recalculation, scores were recomputed for all samples. For each sample, the grade shift (Δ) was defined as the difference

between the baseline score (all donors) and the score with that donor omitted. The 13 shifts were summarized as the median absolute shift (median |Δ|) ± standard deviation (SD) and the maximum absolute shift (max |Δ|) in points. Prespecified stability targets were median |Δ| ≤ 0.20 and max |Δ| ≤ 1.00 points. Results are presented for healthy donors (anchor sensitivity) and for patients (score stability).

2.6.2. Bootstrap of anchors

To quantify sampling uncertainty in the anchor estimates (per-marker $P90$ from the 13 healthy donors), bootstrap resampling of the donor set was performed. 1000 bootstrap datasets were generated by sampling donors with replacement; each dataset contained 13 draws from the original donor pool, allowing any donor to appear zero, once, or multiple times while preserving sample size. For each bootstrap dataset, per-marker anchors were recomputed and CAR-Cytotox scores were recalculated for all samples. For each patient, the bootstrap score distribution was summarized by the mean, SD, and the 95% confidence interval (CI) defined by the 2.5th and 97.5th percentiles of the bootstrap distribution. Our prespecified criterion was a CI width < 2.0 points. We also examined whether bootstrap grades remained in the same band as the baseline grade (low, moderate, or high).

2.6.3. Delete-3 test

To evaluate robustness of the score, a Delete-3 stress test was performed. Patient scores were recalculated 300 times. In each calculation, a random triplet of healthy donors was removed, leaving a 10-donor subset. For each calculation, per-marker $P90$ anchors were recomputed from this subset and CAR-Cytotox scores were recalculated. For each patient, grades across calculations were summarized by the minimum, mean, maximum, and standard deviation (points), and notations were made whether grades remained in the same prespecified band as the baseline grade (low, moderate, or high).

2.7. Development of the online CAR-Cytotox calculator

A web-based calculator (HTML/CSS/JavaScript) implementing the CAR-Cytotox scoring algorithm described in this article was developed to provide researchers and clinicians worldwide with a convenient means to compute the CAR-Cytotox score quickly and reproducibly. Anchor values for normalization were fixed to the 90th percentile of each marker derived from the healthy-donor reference dataset. The interface accepts per-marker readouts as fold change values for flow cytometry and multiplex bead-based immunoassays, and as $2^{-\Delta\Delta Ct}$ for RT-qPCR. Missing inputs are excluded from the calculation and the partial sum is proportionally rescaled to the 0–10 range. A notification is displayed indicating which values are missing and advising that results should be interpreted with caution. All computations run client-side with no data storage or transmission. The calculator is deployed as a static webpage (GitHub Pages, GitHub, Inc., USA).

3. Results

Thirteen healthy donors (46% female, 54% male, aged 27–63 years, median 51 years) and three patients with newly diagnosed ALL (ages 75, 59, and 66 years) were enrolled. For each participant, CAR T cell products were manufactured, stimulated with CD19-coated beads, and assessed by flow cytometry (CD107a), RT-qPCR (cytotoxicity-related transcripts), and a multiplex bead-based immunoassay (supernatants). Among healthy donors, mean transduction efficiency within T lymphocytes ($CD4^+$ and $CD8^+$) was 46.7 ± 3.4%. Higher CAR expression was observed in $CD4^+$ T cells (52.1 ± 4.0%) compared with $CD8^+$ T cells (34.4 ± 3.6%). In patients, CAR^+ cells were observed in 60%, 44.6% and 37.8% within T lymphocytes ($CD4^+$ and $CD8^+$). Higher CAR expression was observed in $CD4^+$ T cells (60.4%, 46.5%, 40.3%) compared with $CD8^+$ T cells (54.8%, 30.9%, 18.2%), consistent with results observed in healthy donors.

3.1. Flow cytometry (CD107a degranulation)

Degranulation (CD107a) was quantified within $CD8^+$ CAR^+ T cells after 48 hours of stimulation with CD19-coated beads. Among healthy donors (n = 13), the mean frequency of $CD107a^+$ cells within $CD8^+$ CAR^+ T cells increased from 17.0 ± 1.2% (mean ± SEM) in unstimulated controls to 25.7 ± 2.5% after stimulation, an absolute mean increase of 8.8 percentage points (paired t-test, p = 0.0006), corresponding to a mean fold change of 1.50. In patients, stimulated $CD107a^+$ frequencies were 19.4%, 18.0%,

and 36.9%, while matched unstimulated controls were 13.8%, 11.8%, and 12.1%, corresponding to absolute increases of 5.6, 6.2, and 24.8 percentage points and fold changes (stimulated over unstimulated) of 1.41, 1.53, and 3.05, respectively. CAR-related degranulation was observed in all patient samples. The gating strategy and the summary of results are shown in Fig. 1.

Insert Fig. 1 *about here.*

3.2. RT–qPCR of cytotoxicity-related transcripts

Relative expression of the selected transcripts (*BCL2, DOCK8, FHL3, GZMB, ITGB1, NKG7, PRF1, STX11, UNC13D*) was calculated by the $2^{-\Delta\Delta Ct}$ method using *HPRT1* as the endogenous control and the unstimulated condition as the calibrator. Among healthy donors (n = 13), only *BCL2* (adjusted p = 0.0237) and *GZMB* (adjusted p = 0.0078) showed statistically significant changes after CD19-bead stimulation based on a one-way ANOVA with Dunnett multiple comparisons test. All other transcripts did not reach the significance threshold (p ≥ 0.05). For *BCL2*, the mean fold change was 1.966 ± 0.393 (mean ± SEM), representing an increase of 0.966 from the unstimulated condition. For *GZMB*, the mean fold change was 2.084 ± 0.298, representing an increase of 1.084 from the unstimulated condition. Similarly, in patient samples, only *BCL2* and *GZMB* showed notable increases. *BCL2* fold changes were 1.187, 2.966, and 1.631, with increases of 0.187, 1.966, and 0.631 from the unstimulated condition. *GZMB* fold changes were 0.894, 3.443, and 3.157, with changes of − 0.106, 2.443, and 2.157, respectively. Overall, patient results closely mirrored those of healthy donors, with elevations confined to *BCL2* and *GZMB* and minimal changes in the remaining transcripts. Summary of results is shown in Fig. 2, and complete transcript fold changes, means ± SEM, and adjusted p values for donors (n = 13) and patients (n = 3) are provided in Supplementary Table S1.

Insert Fig. 2 *about here.*

3.3. Multiplex bead-based immunoassay

Analytes (IL-4, IL-6, IL-10, IL-17A, TNF-α, IFN-γ, soluble Fas, FasL, granzyme A, granzyme B, perforin, granulysin) were quantified in supernatants collected after 48 hours of CD19-coated bead stimulation of CAR T cells using the LEGENDplex assay. In healthy donors (n = 13), stimulation resulted in significant increases in IL-4 (adjusted p = 0.036), IL-6 (adjusted p = 0.026), FasL (adjusted p = 0.011), and IFN-γ (adjusted p = 0.040) based on a paired t-test with Šidák-Bonferroni correction. All other analytes did not reach the significance threshold (p ≥ 0.05). For IL-4, stimulated and unstimulated means were 15.56 ± 1.68 (mean ± SEM) and 11.56 ± 1.33 pg/mL, with an absolute mean increase of 3.993 pg/mL and a 1.35 fold change. For IL-6, stimulated and unstimulated means were 54.08 ± 11.92 and 19.67 ± 8.91 pg/mL, with an absolute mean increase of 34.41 pg/mL and a 2.75 fold change. For FasL, stimulated and unstimulated means were 108.4 ± 11.87 and 75.66 ± 6.35 pg/mL, with an absolute mean increase of 32.72 pg/mL and a 1.43 fold change. For IFN-γ, stimulated and unstimulated means were 8652 ± 2111.6 and 2235 ± 689.85 pg/mL, with an absolute mean increase of 6417 pg/mL and a 3.87 fold change. In patients, similar trends were observed. For IL-4, fold changes (stimulated over unstimulated) were 1.21, 3.99, and 1.83; for IL-6 1.38, 5.04, and 3.65; for FasL 1.30, 1.64, and 1.51; and for IFN-γ 2.77, 4.78, and 1.51. Summary of results is shown in Fig. 3, and complete analyte concentrations, fold changes, and adjusted p values for donors (n = 13) and patients (n = 3) are provided in Supplementary Table S2.

Insert Fig. 3 *about here.*

3.4. CAR-Cytotox score

We developed a 0–10 CAR-Cytotox scoring system to quantify CAR-related cytotoxicity. Among the analyzed readouts, CD107a measured by flow cytometry showed a significant increase upon CD19 stimulation (p = 0.0006) and was assigned a weight of 3 points. In the gene expression analysis, *BCL2* (p = 0.0237) and *GZMB* (p = 0.0078) showed statistically significant differences compared to the unstimulated condition, and were assigned weights of 1 and 2 points, respectively. In the multiplex bead-based immunoassay, IL-4, IL-6, FasL, and IFN-γ were significantly different from the unstimulated condition (0.05 ≥ p > 0.01), each receiving a weight of 1 point. The 90th percentile ($P90$) of healthy donor values was calculated for all selected markers and served as the upper anchor for score normalization, while FC = 1 (no change from the unstimulated condition) served as the lower anchor. $P90$ reference values for each marker are shown in Table 2. Normalized contributions (N) were calculated for

each marker and multiplied by their respective weights. Weighted normalized contributions were summed to yield the final CAR-Cytotox score, ranging from 0 (no cytotoxicity) to 10 (very high cytotoxicity).

Table 2
Ninetieth percentile ($P90$) values of healthy donor marker readouts (n = 13) used as reference upper anchors in CAR-Cytotox score scaling.

	CD107a	*BCL2*	*GZMB*	IL-4	IL-6	FasL	IFN-γ
***P*90 fold change**	1.95	3.96	3.46	1.78	12.48	1.79	17.27

The mean CAR-Cytotox score for healthy controls was 4.53 ± 0.66 (mean ± SEM). The three patient samples yielded scores of 2.14, 6.70, and 7.38 points, respectively. Based on the predefined interpretation bands, the first patient's score fell within the low cytotoxicity range (0–3), while the latter two exhibited high cytotoxicity (6–10). Detailed CAR-Cytotox scores for all healthy donors and their interpretations are provided in Supplementary Table S3.

3.5. Score validation

A leave-one-out (LOO) jackknife was applied to evaluate the robustness of the $P90$ anchors and the influence of individual donors on the CAR-Cytotox score. In each of 13 leave-one-out iterations, one healthy donor was omitted, per-marker $P90$ anchors were recomputed, and scores for all samples were recalculated. Across iterations, grade shifts in healthy donors were small overall (median |Δ| ± SD: 0.050 ± 0.222 points). Three donor-wise max |Δ| values exceeded the 1.00-point threshold (1.003, 1.152, 1.170), but these were rare outliers. All other shifts were low, supporting anchor stability. For patients, median |Δ| ± SD were 0.041 ± 0.091, 0.150 ± 0.097, and 0.088 ± 0.203 points (Patients 1–3), with max |Δ| values of 0.317, 0.440, and 0.618 points, respectively. Notably, no decision-band changes occurred in patient samples across all iterations (low, moderate, or high). Overall, results meet the prespecified stability target for median |Δ| (≤ 0.20) and are largely within the max |Δ| criterion (≤ 1.00), indicating a robust scoring framework. Full LOO results are provided in Supplementary Table S4.

Estimating per-marker $P90$ anchors from a finite donor cohort (n = 13) introduces sampling uncertainty. To quantify this and its impact on patient CAR-Cytotox scores, we performed a non-parametric bootstrap (1000 resamples of 13 donors with replacement), recomputed anchors for each resample, and rescored all samples. The bootstrap mean scores were 2.24 for Patient 1 (95% CI 1.84–2.70; width 0.86), 6.81 for Patient 2 (95% CI 6.03–7.74; width 1.71), and 7.52 for Patient 3 (95% CI 6.63–8.48; width 1.85). All CIs were narrower than the prespecified 2.0-point threshold and remained entirely within the same decision bands as the baseline classifications (Patient 1: low, Patients 2–3: high). Bootstrap means differed from baseline scores by ≤ 0.15 points, supporting stable anchors and reliable patient classification.

We performed a Delete-3 test to evaluate score robustness under more severe perturbations, recalculating patient grades 300 times on 10-donor subsets created by randomly deleting three donors. Scores remained stable: Patient 1 ranged 1.98–2.49 (mean 2.20, SD 0.15), Patient 2 6.28–7.64 (mean 6.80, SD 0.33), and Patient 3 7.02–8.35 (mean 7.53, SD 0.37). The corresponding ranges were 0.51, 1.36, and 1.34 points, and mean deviations from the baseline scores were ≤ 0.15 points. No patient crossed a decision-band threshold (Patient 1: low, Patients 2–3: high). Importantly, these ranges were fully contained within the bootstrap 95% CIs and the Delete-3 means were within ≤ 0.05 points of the bootstrap means, demonstrating complete consistency with the bootstrap results and supporting the robustness of the CAR-Cytotox score even when approximately 23% of reference donors were removed.

3.6. Online CAR-Cytotox calculator

The web-based calculator accurately reproduced the CAR-Cytotox scoring algorithm described in this article, yielding results identical to manual calculations. Users enter per-marker fold change values for flow cytometry and multiplex bead-based immunoassay, or $2^{-\Delta\Delta Ct}$ values for RT-qPCR, and receive an overall CAR-Cytotox score within seconds. Calculations execute locally in the browser, and the interface provides immediate feedback if any marker values are missing, applies proportional rescaling, and advises careful interpretation. The output reports the total score and its interpretation according to predefined bands (low, moderate, or high). The calculator is publicly available at https://lsrsen.github.io/CAR-Cytotox/ (accessed October 6, 2025) and functions across major browsers.

4. Discussion

This study establishes and validates a multi-assay framework for quantifying CAR T cell cytotoxicity and translates it into a practical 0–10 CAR-Cytotox score. A score of 0 represents no measurable cytotoxic activity, while a score of 10 indicates high cytotoxic activity. Using standardized CD19-bead stimulation, we observed consistent activation across complementary readouts from flow cytometry, real-time quantitative PCR, and multiplex bead-based immunoassay. Together, these assays capture distinct layers of CAR T cell function, including immediate degranulation, transcriptional programming, and cytokine secretion. The findings were reproducible across 13 healthy donors and mirrored in three B-ALL patients, supporting the validity of the approach.

Transduction efficiency in our study reflected observations from clinical practice, where CAR expression in final products typically ranges between 30% and 60% of T cells (2, 8), with values above 15% considered satisfactory for release (9). In our samples, transduction efficiency was within these ranges and exceeded the 15% benchmark, indicating satisfactory expression levels and favorable transduction conditions. Within the transduced population, CAR expression was higher in $CD4^+$ than in $CD8^+$ T cells in both healthy donors and patients, consistent with previous reports and likely reflecting the greater proliferative capacity of $CD4^+$ cells during culture (2).

CD107a is one of the most established cytotoxicity markers and showed a significant and reproducible increase upon CD19 stimulation, confirming strong degranulation responses (3). However, CD107a exhibited relatively high baseline expression in unstimulated controls, likely reflecting residual activation acquired during cell expansion. This suggests that CD107a surface mobilization can occur independently of CAR engagement and that relying on this marker alone may underestimate CAR-specific degranulation when background levels are elevated. These observations highlight the advantage of the CAR-Cytotox score, which integrates multiple functional readouts to provide a more comprehensive measure of cytotoxic potency.

In RT-qPCR, *GZMB* and *BCL2* were significantly upregulated compared to unstimulated controls. *GZMB*, encoding granzyme B, the key protease driving target-cell apoptosis (10, 11), was expectedly elevated. *BCL2*, typically downregulated during acute activation and upregulated later to sustain survival, was already increased after 48 hours of stimulation. This early rise suggests that effective CAR T cells may rapidly upregulate *BCL2* for pro-survival programming reported to support effector and memory T cells (12, 13). Beyond its canonical anti-apoptotic role, *BCL2* critically regulates intracellular Ca^{2+} homeostasis by modulating Ca^{2+} release from the endoplasmic reticulum and mitochondrial Ca^{2+} uptake, thereby limiting Ca^{2+}-induced mitochondrial dysfunction and activation-induced cell death. Early *BCL2* upregulation may therefore help buffer sustained Ca^{2+} signaling downstream of CAR engagement, enabling prolonged cytotoxic function while preserving cellular viability (14, 15). The lack of upregulation of other transcripts (*DOCK8, FHL3, ITGB1, NKG7, PRF1, STX11, UNC13D*) was somewhat unexpected but explainable based on their activation biology. *DOCK8* and *FHL3* are structural adaptors whose function depends on localization and complex assembly rather than transcriptional induction (16–21). *ITGB1* (β1 integrin) mediates adhesion and immunological synapse stability through affinity and avidity changes rather than through increased gene expression (22, 23). *NKG7* often shows high baseline expression in cytotoxic CAR T cells, leaving little capacity for further induction. Because the protein is granule-associated, degranulation can transiently reduce intracellular *NKG7* signal (24–26). *PRF1* is usually upregulated in activated T cells, so its unchanged level here may reflect timing, culture cytokines, or the already elevated baseline typical for expanded CAR T products (27, 28). *STX11* and *UNC13D* encode key mediators for lytic granule fusion and priming of cytotoxic vesicles at the plasma membrane of the immunological synapse, and their regulation is driven mainly by synaptic recruitment, with only modest or delayed transcriptional changes (29–32). Altogether, these expression patterns indicate that many cytotoxic genes are already highly expressed in the manufactured CAR T cells or that some respond primarily through post-translational mechanisms during acute activation.

In the multiplex bead-based immunoassay, IL-6 and IFN-γ were robustly elevated, representing canonical effector activation (1, 33). IL-4 and FasL were also significantly elevated. The IL-4 increase was somewhat surprising, as IL-4 generally suppresses cytotoxic programs, yet its coinduction here may reflect a transient regulatory phase that coexists with strong effector activity (34, 35). FasL, a ligand stored in secretory lysosomes, is rapidly transported to the plasma membrane during degranulation, explaining its clear increase after stimulation. In contrast, soluble Fas receptor levels remained unchanged, consistent with its slower induction kinetics. The generation of soluble Fas generally occurs later and depends on sustained cytokine signaling and

cell turnover, making stable levels explainable within the 48-hour activation window (10, 36). IL-10, a regulatory cytokine often produced later or by other immune subsets, remained low (37–39). TNF-α, often proposed as a CAR T activation marker (40), was also not increased significantly, suggesting that its peak may occur earlier or during expansion rather than after 48 hours of stimulation and indicating that TNF-α may not be a reliable marker of acute CAR T cell activation in the 48-hour stimulation window. IL-17A, which requires Th17 polarization and cytokines such as IL-6 and TGF-β, remained low, consistent with the Th1-skewed phenotype typical of IL-2 expanded CAR T cells (41–43). Granzyme A, granzyme B, perforin, and granulysin also showed no significant increase, likely reflecting high baseline expression in the IL-2 expanded product, which may have masked additional production during the 48-hour stimulation period. However, cytotoxic activity of CAR T cells was preserved, as evidenced by robust degranulation and cytokine responses (7). These observations highlight that CAR-specific cytotoxic mechanisms differ from those of conventional T cells, and therefore, commonly used T cell activation assays do not always apply. Studies focused directly on CAR T cells, as demonstrated in this study, are needed to identify which markers reliably reflect their effector state and killing capacity.

Although the number of donors and patient samples was limited, multiple robustness and validation analyses supported the stability and reproducibility of the CAR-Cytotox score. Cytotoxicity was assessed using standardized CD19-coated beads rather than live target cells, enabling reproducibility but not fully capturing tumor-specific interactions or resistance mechanisms. In addition, analyses were performed at a single 48-hour time point, which may have missed transient or delayed activation signals. Finally, this study was conducted using a single CD19 CAR construct, and further studies are necessary to confirm the applicability of the CAR-Cytotox score to other constructs, such as CD20 or BCMA.

Integrating all significant readouts, the CAR-Cytotox score combines functional (CD107a), transcriptional (*GZMB, BCL2*), and secreted (IFN-γ, IL-6, IL-4, FasL) markers into a single, interpretable 0–10 scale. Patient samples fell into low or high cytotoxicity bands, indicating that the score captures the expected biological variability across individuals. Robustness testing through leave-one-out, bootstrap, and delete-3 analyses confirmed the stability of percentile anchors and consistent classification despite the limited donor pool. Overall, this framework provides a practical, standardized method for quantifying CAR T cell cytotoxicity. By integrating diverse but complementary assays into one score and implementing it through an open-access web calculator, it offers a reproducible and accessible tool for comparing CAR T products, optimizing manufacturing, and supporting translational research.

5. Conclusions

This study introduces a standardized, multi-assay framework for quantifying CAR T cell cytotoxicity and translates it into a practical 0–10 CAR-Cytotox score. By integrating degranulation (CD107a), transcriptional upregulation (*GZMB*, *BCL2*), and secreted effectors (IFN-γ, IL-4, IL-6, FasL), the score captures distinct functional layers of CAR T cell function and distinguishes biologically diverse responses among donors and patients. Implemented through a web-based open-access calculator, the CAR-Cytotox score offers a reproducible and accessible tool for comparing the functionality of CAR T cell products and supporting translational research.

Declarations

Ethics approval and consent to participate

The study was conducted in accordance with the Declaration of Helsinki and approved by the Ministry of Health of the Republic of Slovenia, National Medical Ethics Committee (approval code: 0120–514/2023/5). Written informed consent was obtained from all participants prior to inclusion in the study.

Consent for publication

All authors have read and approved the final manuscript and consent to its publication.

Conflict of interest

The authors declare no potential conflicts of interest.

Funding

This work was funded by the Slovenian Research Agency (ARIS) under the postgraduate research program and grant number P3-0083.

Author Contribution

LS and AK designed the study. LS, AK, and LJ performed the experiments and analyzed the data. LS wrote the original draft of the manuscript. All authors contributed to the article, reviewed the manuscript, and approved the submitted version.

Acknowledgement

The authors would like to thank the healthy donors and patients who agreed to participate in the study and generously provided samples. The authors acknowledge the use of ChatGPT v5.0 (OpenAI, USA) to assist in the design and development of the web-based calculator. The tool was used for technical support only and did not contribute to data analysis, interpretation of results, or scientific conclusions.

Data Availability

The data supporting the findings of this study are available from the corresponding author upon reasonable request. Additional information supporting the conclusions of this article is provided in the supplementary material. The CAR-Cytotox calculator is freely available at [https://lsrsen.github.io/CAR-Cytotox/](https:/lsrsen.github.io/CAR-Cytotox) .

References

1. Kiesgen, S., Messinger, J. C., Chintala, N. K., Tano, Z. & Adusumilli, P. S. Comparative analysis of assays to measure CAR T-cell-mediated cytotoxicity. *Nat. Protoc.* **16** (3), 1331–1342 (2021).
2. Jackson, Z. et al. Automated Manufacture of Autologous CD19 CAR-T Cells for Treatment of Non-hodgkin Lymphoma. *Front. Immunol.* **11**, 1941 (2020).
3. Levstek, L., Janžič, L., Ihan, A. & Kopitar, A. N. Biomarkers for prediction of CAR T therapy outcomes: current and future perspectives. *Front. Immunol.* ;**15**. (2024).
4. Wang, Z. et al. 3D live imaging and phenotyping of CAR-T cell mediated-cytotoxicity using high-throughput Bessel oblique plane microscopy. *Nat. Commun.* **15** (1), 6677 (2024).
5. Pipkin, M. E., Rao, A. & Lichtenheld, M. G. The transcriptional control of the perforin locus. *Immunol. Rev.* **235** (1), 55–72 (2010).
6. Dirar, Q. et al. Activation and degranulation of CAR-T cells using engineered antigen-presenting cell surfaces. *PLoS One*. **15** (9), e0238819 (2020).
7. Tamang, D. L. et al. Induction of granzyme B and T cell cytotoxic capacity by IL-2 or IL-15 without antigens: multiclonal responses that are extremely lytic if triggered and short-lived after cytokine withdrawal. *Cytokine* **36** (3–4), 148–159 (2006).
8. Palani, H. K. et al. Safety, efficacy and total cost of point-of-care manufactured anti-CD19 CAR-T cell therapy in India: VELCART trial. *Mol. Ther. Oncol.* **33** (2), 200977 (2025).
9. Distributive Manufacturing of CD19 CAR-T Cells Using CliniMACS Prodigy. Feasibility and Real-World Experience from India [Internet]. (2022).

10. Montalvo, M. J. et al. Decoding the mechanisms of chimeric antigen receptor (CAR) T cell-mediated killing of tumors: insights from granzyme and Fas inhibition. *Cell. Death Dis.* **15** (2), 109 (2024).
11. Li, J. et al. Granzymes expression patterns predict immunotherapy response and identify the heterogeneity of CD8 + T cell subsets. *Cancer Biomark.* **38** (1), 77–102 (2023).
12. Wang, H. et al. Bcl-2 Enhances Chimeric Antigen Receptor T Cell Persistence by Reducing Activation-Induced Apoptosis. *Cancers (Basel)* ;**13**(2). (2021).
13. Lee, Y. G. et al. Modulation of BCL-2 in Both T Cells and Tumor Cells to Enhance Chimeric Antigen Receptor T-cell Immunotherapy against Cancer. *Cancer Discov*. **12** (10), 2372–2391 (2022).
14. Vervliet, T., Parys, J. B. & Bultynck, G. Bcl-2 proteins and calcium signaling: complexity beneath the surface. *Oncogene* **35** (39), 5079–5092 (2016).
15. Rong, Y. & Distelhorst, C. W. Bcl-2 protein family members: versatile regulators of calcium signaling in cell survival and apoptosis. *Annu. Rev. Physiol.* **70**, 73–91 (2008).
16. Xu, X. et al. LRCH1 interferes with DOCK8-Cdc42-induced T cell migration and ameliorates experimental autoimmune encephalomyelitis. *J. Exp. Med.* **214** (1), 209–226 (2017).
17. Samson, T. et al. The LIM-only proteins FHL2 and FHL3 interact with alpha- and beta-subunits of the muscle alpha7beta1 integrin receptor. *J. Biol. Chem.* **279** (27), 28641–28652 (2004).
18. Coghill, I. D. et al. FHL3 is an actin-binding protein that regulates alpha-actinin-mediated actin bundling: FHL3 localizes to actin stress fibers and enhances cell spreading and stress fiber disassembly. *J. Biol. Chem.* **278** (26), 24139–24152 (2003).
19. Kearney, C. J., Randall, K. L. & Oliaro, J. DOCK8 regulates signal transduction events to control immunity. *Cell. Mol. Immunol.* **14** (5), 406–411 (2017).
20. Randall, K. L. et al. DOCK8 deficiency impairs CD8 T cell survival and function in humans and mice. *J. Exp. Med.* **208** (11), 2305–2320 (2011).
21. Sun, X. et al. Mechanosensing through Direct Binding of Tensed F-Actin by LIM Domains. *Dev. Cell.* **55** (4), 468–82e7 (2020).
22. Chigaev, A. et al. Real time analysis of the affinity regulation of alpha 4-integrin. The physiologically activated receptor is intermediate in affinity between resting and Mn(2+) or antibody activation. *J. Biol. Chem.* **276** (52), 48670–48678 (2001).
23. Doucey, M. A. et al. The beta1 and beta3 integrins promote T cell receptor-mediated cytotoxic T lymphocyte activation. *J. Biol. Chem.* **278** (29), 26983–26991 (2003).
24. Ng, S. S. et al. The NK cell granule protein NKG7 regulates cytotoxic granule exocytosis and inflammation. *Nat. Immunol.* **21** (10), 1205–1218 (2020).
25. Lelliott, E. J. et al. NKG7 Enhances CD8 + T Cell Synapse Efficiency to Limit Inflammation. *Front. Immunol.* **13**, 931630 (2022).
26. Chen, Y. et al. Ectopic expression of NKG7 enhances CAR-T function and improves the therapeutic efficacy in liquid and solid tumors. *Pharmacol. Res.* **210**, 107506 (2024).
27. Ishii, K. et al. Perforin-deficient CAR T cells recapitulate late-onset inflammatory toxicities observed in patients. *J. Clin. Invest.* **130** (10), 5425–5443 (2020).
28. Voskoboinik, I., Whisstock, J. C. & Trapani, J. A. Perforin and granzymes: function, dysfunction and human pathology. *Nat. Rev. Immunol.* **15** (6), 388–400 (2015).
29. Hong, W. Cytotoxic T lymphocyte exocytosis: bring on the SNAREs! *Trends Cell. Biol.* **15** (12), 644–650 (2005).
30. Dabrazhynetskaya, A. et al. Syntaxin 11 marks a distinct intracellular compartment recruited to the immunological synapse of NK cells to colocalize with cytotoxic granules. *J. Cell. Mol. Med.* **16** (1), 129–141 (2012).
31. D'Orlando, O. et al. Syntaxin 11 is required for NK and CD8$^+$ T-cell cytotoxicity and neutrophil degranulation. *Eur. J. Immunol.* **43** (1), 194–208 (2013).
32. Wang, J. et al. T Cell Defects: New Insights Into the Primary Resistance Factor to CD19/CD22 Cocktail CAR T-Cell Immunotherapy in Diffuse Large B-Cell Lymphoma. *Front. Immunol.* **13**, 873789 (2022).

33. Sršen, L. et al. CAR T therapy in adult DLBCL patients in Slovenia: Evaluation of predictive scores for outcomes and adverse events. *Hum. Vaccin Immunother*. **22** (1), 2620889 (2026).
34. Bratke, K. et al. Interleukin-4 suppresses the cytotoxic potential of in vitro generated, adaptive regulatory CD4 T cells by down-regulation of granzyme B. *Immunology* **127** (3), 338–344 (2009).
35. Silveira, C. R. F. et al. Cytokines as an important player in the context of CAR-T cell therapy for cancer: Their role in tumor immunomodulation, manufacture, and clinical implications. *Front. Immunol.* **13**, 947648 (2022).
36. Yi, F. et al. CAR-engineered lymphocyte persistence is governed by a FAS ligand-FAS autoregulatory circuit. *Nat. Cancer*. **6** (10), 1638–1655 (2025).
37. Zhao, Y. et al. IL-10-expressing CAR T cells resist dysfunction and mediate durable clearance of solid tumors and metastases. *Nat. Biotechnol.* **42** (11), 1693–1704 (2024).
38. Jankovic, D., Kugler, D. G. & Sher, A. IL-10 production by CD4 + effector T cells: a mechanism for self-regulation. *Mucosal Immunol.* **3** (3), 239–246 (2010).
39. Morris, E. C., Neelapu, S. S., Giavridis, T. & Sadelain, M. Cytokine release syndrome and associated neurotoxicity in cancer immunotherapy. *Nat. Rev. Immunol.* **22** (2), 85–96 (2022).
40. Harari-Steinfeld, R., Abhinav Ayyadevara, V. S. S., Cuevas, L., Marincola, F. & Roh, K. H. Standardized in-vitro evaluation of CAR-T cells using acellular artificial target particles. *Front. Immunol.* **13**, 994532 (2022).
41. Guedan, S. et al. ICOS-based chimeric antigen receptors program bipolar TH17/TH1 cells. *Blood* **124** (7), 1070–1080 (2014).
42. Harbour, S. N. et al. T(H)17 cells require ongoing classic IL-6 receptor signaling to retain transcriptional and functional identity. *Sci. Immunol.* ;**5**(49). (2020).
43. Majchrzak, K. et al. Exploiting IL-17-producing CD4 + and CD8 + T cells to improve cancer immunotherapy in the clinic. *Cancer Immunol. Immunother*. **65** (3), 247–259 (2016).

Figures

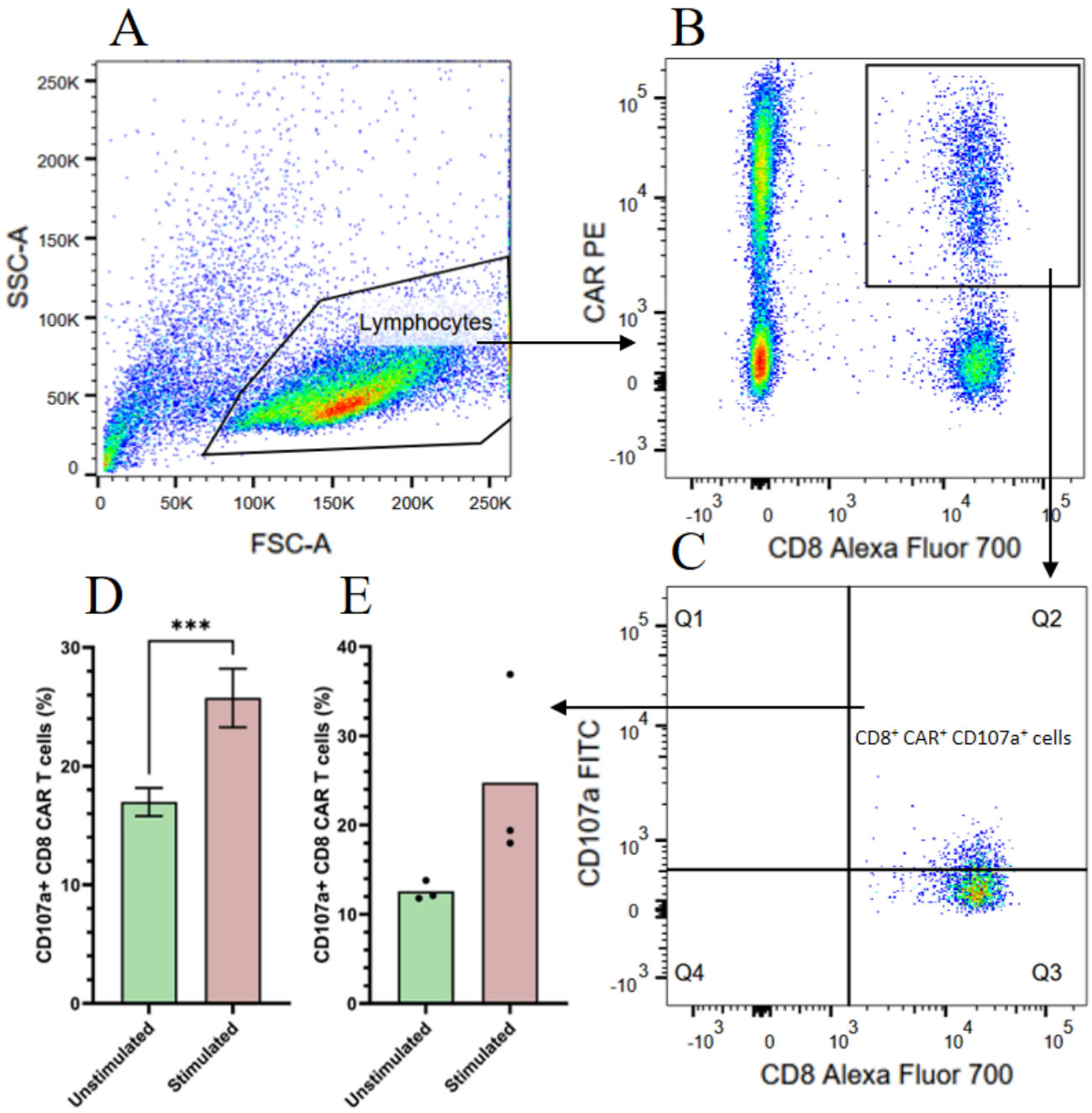


Figure 1

Flow cytometry gating strategy to determine $CD8^+$ CAR^+ $CD107a^+$ cells and CD107a degranulation of CD19-stimulated CAR T cells. (A) Lymphocytes were gated by FSC-A/SSC-A. (B) Within lymphocytes, $CD8^+$ CAR^+ T lymphocytes were identified. (C) Degranulation was quantified as CD107a expression within $CD8^+$ CAR^+ T cells. (D) Summary for healthy donors (n = 13) and (E) for patients, shown as a bar plot of the frequency of $CD107a^+$ cells among $CD8^+$ CAR^+ T lymphocytes after 48 hours of stimulation with CD19-coated beads versus unstimulated control; bars represent mean ± SEM for healthy donors and bars with individual values for patients; significance was computed for healthy donors by paired t-test, ***$p < 0.001$.

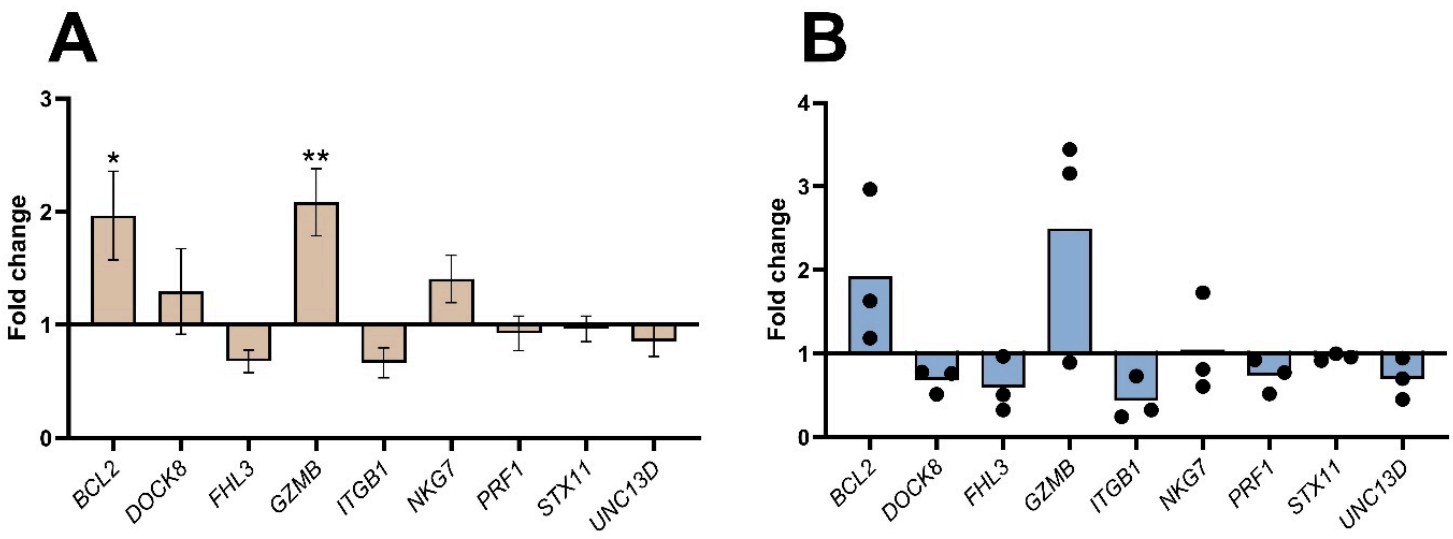


Figure 2

Fold change in gene expression, analyzed by quantitative real-time PCR. Bar graphs show the relative mRNA expression (fold change) of selected genes in stimulated CAR T cells compared to unstimulated CAR T cells in (A) healthy donors and (B) patients. Data for healthy donors are presented as mean ± SEM (n = 13), and for patients as mean with individual values. Statistically significant differences in healthy donors were determined by one-way ANOVA followed by post-hoc Dunett's multiple comparisons test, where *p ≤ 0.05 and **p ≤ 0.01.

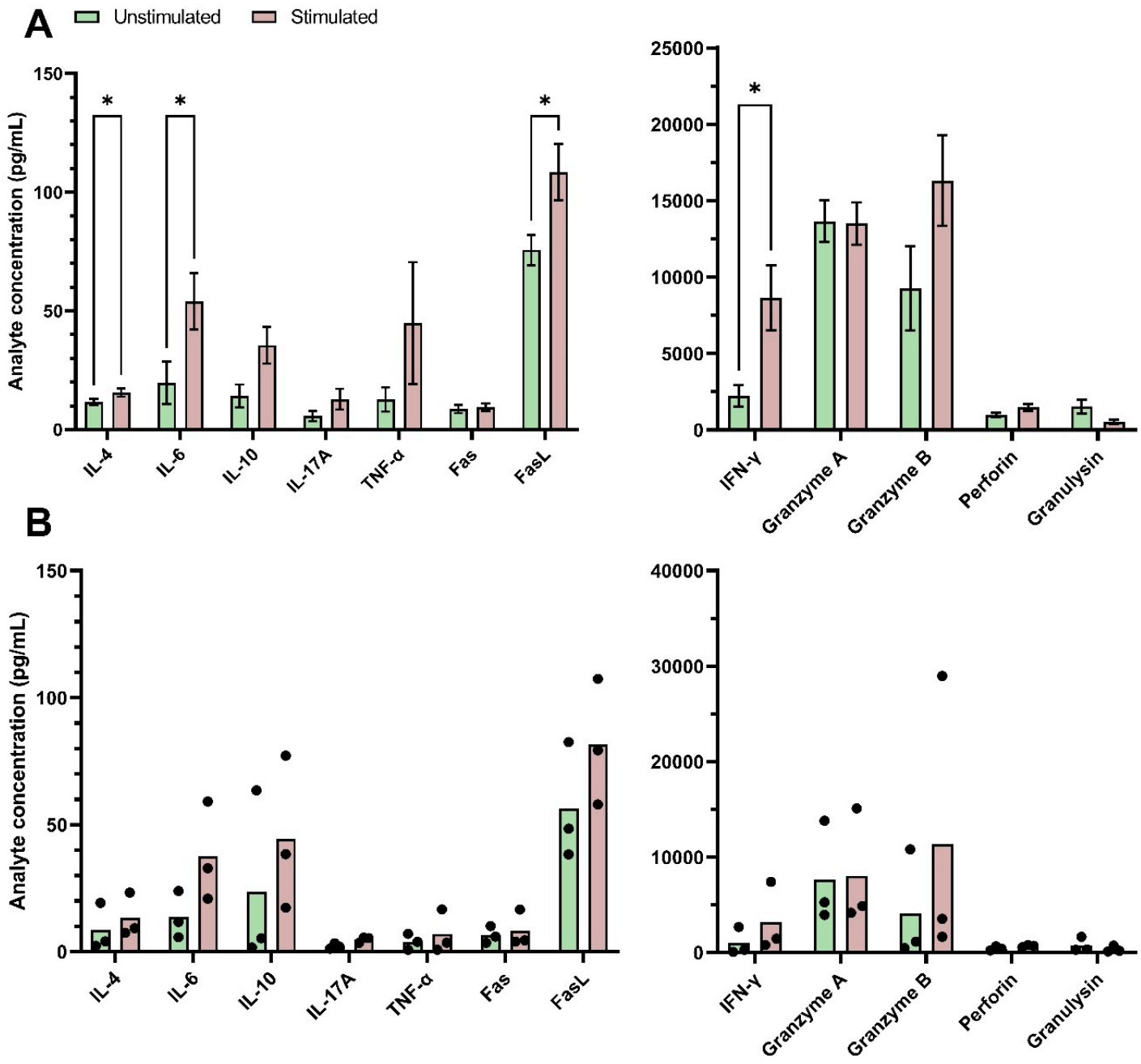


Figure 3

Analyte concentrations in supernatants of unstimulated and stimulated CAR T cells from (A) healthy donors and (B) patients, measured using the BioLegend LEGENDplex multiplex bead-based immunoassay. Bar graphs display the mean ± SEM (n = 13) for healthy donors and mean with individual values for patients. Statistical analysis of healthy donor results was performed using a parametric paired t-test, with correction for multiple comparisons using the Šidák-Bonferroni *post-hoc* test (*p ≤ 0.05).

Supplementary Files

This is a list of supplementary files associated with this preprint. Click to download.

- SUPPLEMENTARY.docx